J|A|C|S COMMUNICATIONS

Published on Web 08/25/2010

Energy Transfer Dynamics in Metal−Organic Frameworks

Caleb A. Kent, Brian P. Mehl, Liqing Ma, John M. Papanikolas,* Thomas J. Meyer,* and Wenbin Lin*

Department of Chemistry, CB#3290, University of North Carolina, Chapel Hill, North Carolina 27599

Received April 2, 2010; E-mail: wlin@unc.edu; tjmeyer@unc.edu; john_papanikolas@unc.edu

Abstract: Isomorphous metal−organic frameworks (MOFs) based on $\{M[4,4'\text{-}(HO_2C)_2\text{-}bpy]_2bpy\}^{2+}$ building blocks (where M = Ru or Os) were designed and synthesized to study the classic Ru to Os energy transfer process that has potential applications in light-harvesting with supramolecular assemblies. The crystalline nature of the MOFs allows precise determination of the distances between metal centers by X-ray diffraction, thereby facilitating the study of the Ru→Os energy transfer process. The mixed-metal MOFs with 0.3, 0.6, 1.4, and 2.6 mol % Os doping were also synthesized in order to study the energy transfer dynamics with a two-photon excitation at 850 nm. The Ru lifetime at 620 nm decreases from 171 ns in the pure Ru MOF to 29 ns in the sample with 2.6 mol % Os doping. In the mixed-metal samples, energy transfer was observed with an initial growth in Os emission corresponding with the rate of decay of the Ru excited state. These results demonstrate rapid, efficient energy migration and long distance transfer in isomorphous MOFs.

The light-harvesting antenna of an artificial photosynthetic device must efficiently collect sunlight and transport the energy to catalytic centers for solar fuel production. The pigment−protein complexes in nature set a high standard by delivering energy from greater than 95% of the absorbed photons to the reaction center.[1] Efficient artificial light-harvesting systems have been actively pursued, including covalently linked porphyrins[2] and metal complex polymers and dendrimers.[3] Self-assembled supramolecular systems are particularly promising because of ease of fabrication and the ability to control macroscopic order through noncovalent interactions.[4]

Energy flow from polypyridyl-based metal-to-ligand charge transfer (MLCT) excited states of Ru^{II} to Os^{II} has provided a useful probe for understanding energy transfer dynamics in ligand-bridged complexes and hydrogen-bonded supramolecular assemblies,[5] functionalized polymers,[6] rigid media,[7] and crystalline molecular solids[8] and across semiconductor interfaces.[9] Metal−organic frameworks (MOFs) have recently emerged as a new class of hybrid materials that can be constructed from a variety of functional building blocks.[10] Photoactive MOFs have been designed for nonlinear optics,[11] luminescence molecular sensing,[12] and bioimaging.[13] The ability to fine-tune molecular building blocks in MOFs makes them an ideal model system for studying energy transfer dynamics in the ordered solid state. Compared to the energy transfer systems that have been examined earlier, well-defined MOF structures can simplify data analysis, allowing the delineation of structure/property relationships to provide important insights into optimizing energy migration and transfer efficiency in artificial light-harvesting systems. We report here the development of isomorphous MOFs based on photoactive $\{M[4,4'\text{-}(HO_2C)_2\text{-}bpy]_2bpy\}^{2+}$ building blocks (where M = Ru or Os) that are linked through zinc−carboxylate bonds. Importantly, by studying energy transfer dynamics in the MOFs with mixed Ru and Os building blocks, we demonstrate the existence of facile intersite and long-range energy transfer in these structurally defined and strongly bonded crystalline solids.

Scheme 1

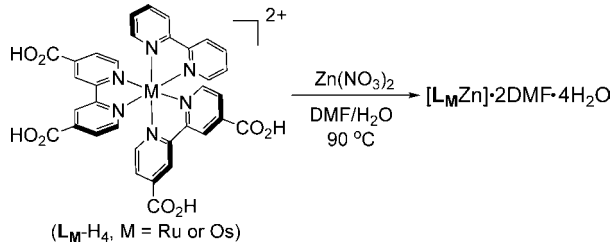

The Ru and Os complexes $\{M[4,4'\text{-}(HO_2C)_2\text{-}bpy]_2bpy\}(PF_6)_2$ ($[\mathbf{L_M}\text{-}H_4](PF_6)_2$) were synthesized by allowing $M[4,4'\text{-}(EtO_2C)_2\text{-}bpy]_2Cl_2$ to react with 2,2′-bipyridine (bpy) followed by acid-catalyzed hydrolysis and anion exchange. The $[\mathbf{L_M}\text{-}H_4](PF_6)_2$ complexes were characterized by NMR spectroscopy, mass spectrometry, and absorption and emission measurements (Supporting Information).[14] The $\mathbf{L_{Ru}}$Zn MOF of formula $[\mathbf{L_{Ru}}Zn]\cdot 2DMF\cdot 4H_2O$ was synthesized by allowing $Zn(NO_3)_2$ and $[\mathbf{L_{Ru}}\text{-}H_4](PF_6)_2$ to react in a dimethylformamide (DMF) and H_2O mixture at 90 °C for 3 days (Scheme 1). The $\mathbf{L_{Os}}$Zn MOF of formula $[\mathbf{L_{Os}}Zn]\cdot 2DMF\cdot 4H_2O$ was similarly prepared. The Os-doped $\mathbf{L_{xOs}}$Zn MOFs with varying Os-doping levels were prepared by adding a small percentage of $[\mathbf{L_{Os}}\text{-}H_4](PF_6)_2$ to the $Zn(NO_3)_2/[\mathbf{L_{Ru}}\text{-}H_4](PF_6)_2$ mixture during crystal growth. The Os-doping levels in these mixed metal MOFs were precisely determined by inductively coupled plasma-optical emission spectroscopy (ICP-OES). The Os-doping level in the mixed Ru/Os MOFs increases as the amount of the $[\mathbf{L_{Os}}\text{-}H_4](PF_6)_2$ complex in the feed increases (Supporting Information).

The $\mathbf{L_{Ru}}$Zn MOF crystallizes in the monoclinic space group $P2_1/c$, with one $\mathbf{L_{Ru}}$ ligand, one Zn atom, and two DMF and four H_2O molecules in the asymmetric unit. The Zn center adopts a tetrahedral geometry by coordinating to four oxygen atoms of four carboxylate groups of the $\mathbf{L_{Ru}}$ ligand, forming a 2D bilayer structure (Figure 1a−c). The distance between the two Ru planes within the bilayer is 10.2 Å, while the distance between Zn planes is 6.8 Å. The resulting 2D layers pack along the *a* axis with the close distance of 4.0 Å between Ru planes of adjacent bilayers. The phase purity of the $\mathbf{L_{Ru}}$Zn MOF was confirmed by comparing the powder X-ray diffraction (PXRD) patterns of the pristine sample and the simulated pattern from the crystal structure. $\mathbf{L_{Os}}$Zn MOF and Os-doped $\mathbf{L_{xOs}}$Zn MOFs are isostructural with the $\mathbf{L_{Ru}}$Zn MOF based on the similarity of their PXRD patterns (Figure 2a). The formulation of the $[\mathbf{L_{Ru}}Zn]\cdot 2DMF\cdot 4H_2O$ MOF was confirmed by thermogravimetric analysis (TGA) which showed 77.8% weight loss (calcd 79.1%) in the 50−400 °C temperature range for the solvent molecules and organic ligands.

Diffuse reflectance UV−vis measurements showed a broad MLCT absorption band between 400 and 600 nm for the $\mathbf{L_{Ru}}$Zn MOF consistent with λ_{max} = 473 nm for $[\mathbf{L_{Ru}}\text{-}H_4](PF_6)_2$in MeOH. The $\mathbf{L_{Os}}$Zn MOF exhibits a broad ^{1}MLCT absorption band between 400 and 650 nm and an absorption band at 710 nm of ∼1/3 the absorptivity arising from the partly spin-allowed "S→T" absorption to ^{3}MLCT with enhanced intensity due to spin−orbit coupling at Os(III) ($\xi(Os^{III}) \approx 3000\ cm^{-1}$).[15] In Figure

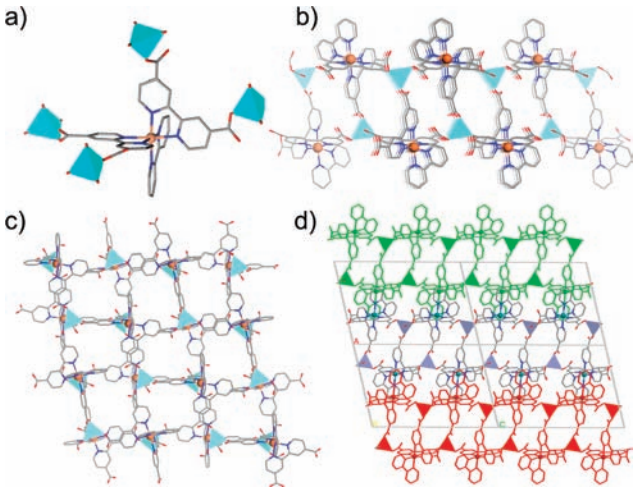

Figure 1. (a) Stick/polyhedra model showing the connectivity of $\mathbf{L_{Ru}}$ and Zn centers in the $\mathbf{L_{Ru}}$Zn MOF. (b) A side view of a 2D bilayer of the $\mathbf{L_{Ru}}$Zn MOF packed along the *b* axis. (c) A top view of the 2D bilayer structure of the $\mathbf{L_{Ru}}$Zn MOF along the *a* axis. (d) A view of the packing of 2D bilayers along the *b* axis.

2b are shown normalized steady state emission spectra for both the $\mathbf{L_{Ru}}$Zn MOF ($\lambda_{max} \approx 620$ nm) and $\mathbf{L_{Os}}$Zn MOF ($\lambda_{max} \approx 720$ nm). As expected, the $\mathbf{L_{Os}}$Zn MOF is significantly less emissive due to enhanced nonradiative decay resulting from the decreased energy gap and higher spin−orbit coupling.[15,16] MOF emission transients were collected on a coupled microscope-time correlated single photon collection system. Two-photon absorption at 850 nm from an ultrafast mode-locked Ti:sapphire laser was used for direct MLCT excitation at Ru^{II}.[17] All MOF samples were flame-sealed into capillary tubes under nitrogen. Lifetimes are reported as averages of values collected at a series of locations in multiple crystals. Variations in lifetimes of ∼20% were observed between different locations and different crystals.

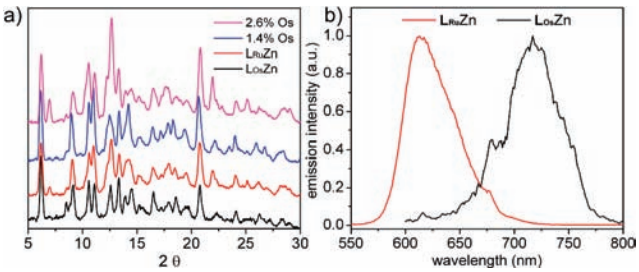

Figure 2. (a) PXRD patterns showing the isostructural nature of $\mathbf{L_{Ru}}$Zn, Os-doped $\mathbf{L_{Ru}}$Zn, and $\mathbf{L_{Os}}$Zn MOFs. (b) Uncorrected normalized steady-state emission spectra of the $\mathbf{L_{Ru}}$Zn MOF and the $\mathbf{L_{Os}}$Zn MOFs.

In Figure 3a are shown emission transients for $\mathbf{L_{Ru}}$Zn (620 nm) and $\mathbf{L_{Os}}$Zn (710 nm) MOFs. The decay profiles for the $\mathbf{L_{Ru}}$Zn and $\mathbf{L_{Os}}$Zn MOFs as well as for the mixed Ru/Os MOFs (Supporting Information) at varying Os-doping levels were nonexponential and could be satisfactorily fit to biexponential kinetics (eq 1). The components of the fit are shown in Table 1.

$$f(t) = Ae^{-(t/\tau_1)} + Be^{-(t/\tau_2)} \quad (1)$$

The observation of multiple decay components in the photoluminescence from pure Ru MOFs is counter to observations in fluid solution, where the luminescence decay is typically single-exponential. Triplet−triplet annihilation could account for the biexponential behavior; however, experiments performed at a series of excitation intensities show no evidence for intensity-dependent effects. The decay kinetics of the Ru^{II}* emission

Table 1. Lifetimes of Os Doped $\mathbf{L_{Ru}}$Zn MOF with Varying Amounts of the $\mathbf{L_{Os}}$ Complex[a]

sample	mol %Os	amplitude$_1$	τ_1 (ns)	amplitude$_2$	τ_2 (ns)
$\mathbf{L_{Ru}}$Zn	0	0.41 ± 0.03	171 ± 30	0.59 ± 0.03	38 ± 7
$\mathbf{L_{0.3Os}}$Zn	0.3	0.38 ± 0.04	135 ± 31	0.62 ± 0.04	25 ± 6
$\mathbf{L_{0.6Os}}$Zn	0.6	0.37 ± 0.03	83 ± 9	0.63 ± 0.03	21 ± 3
$\mathbf{L_{1.4Os}}$Zn	1.4	0.36 ± 0.03	57 ± 10	0.64 ± 0.03	13 ± 2
$\mathbf{L_{2.6Os}}$Zn	2.6	0.37 ± 0.03	29 ± 4	0.63 ± 0.03	5 ± 1
$\mathbf{L_{Os}}$Zn	100	0.40 ± 0.02	8 ± 1	0.60 ± 0.02	1 ± 0.3

[a] Data were taken from multiple crystals in each sample. Lifetime measurements of $\mathbf{L_{Ru}}$Zn MOF and Os-doped samples were taken at 620 nm and $\mathbf{L_{Os}}$Zn MOF at 710 nm.

exhibit a clear detection wavelength dependence, with longer wavelengths showing slower decay rates. Time-dependent emission spectra reconstructed from a series of transients obtained at different wavelengths (Figure 4) show that the biexponential kinetics arises (at least in part) from a time-dependent shift of the emission band. The Ru emission band, which at the earliest observation time has $\lambda_{max} = 612$ nm, shifts by ∼15−20 nm to the red following photoexcitation. Similar red shifts have been observed, in metal complex derivatized polymers,[7a] in electropolymerized thin films,[7c] and on surfaces,[7d] where they were attributed to intersite energy transfer to lower energy trap sites that dominate excited state decay due their decreased energy gaps. Measurements performed at the red edge of the emission band (∼700 nm) yield a Ru^{II}* lifetime of ∼375 ns. The trap sites in the MOFs may be a result of crystal defects during growth, surface sites, or lattice distortion upon solvent removal. While the data presented represent observations obtained at a single site, examination of other sites within the same crystal and measurements performed on other crystals produced qualitatively similar results.

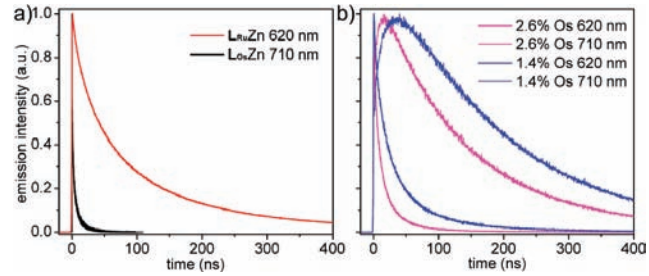

Figure 3. (a) Transient emission decay profiles for $\mathbf{L_{Ru}}$Zn and $\mathbf{L_{Os}}$Zn MOFs monitored at 620 and 710 nm respectively following two-photon excitation at 850 nm. (b) Transients for 1.4 and 2.6 mol % Os-doped $\mathbf{L_{Ru}}$Zn MOFs at 620 and 710 nm with emission at 620 nm dominated by Ru^{II}* and at 710 nm by Os^{II}*.

We have obtained direct evidence for site-to-site energy transfer in mixed Ru^{II}−Os^{II} MOFs (Figure 3b). First, detection of the Os emission in the mixed Ru^{II}−Os^{II} systems at 710 nm shows a delayed growth in the first 10−40 ns that is attributable to Ru^{II}*−Ru^{II} energy migration followed by energy transfer to a lower energy Os "trap site". The growth is fastest for the highest Os-doped sample (2.6 mol %), consistent with a shorter migration distance to the Os^{II} trap, implying that within the initial growth period the excited state makes multiple Ru to Ru hops. In addition, the delayed rise in the Os^{II}* emission at 710 nm coincides with the decay of Ru^{II}* emission detected at 620 nm, which becomes faster as the Os^{II} doping level is increased (Figure 3b). Data taken from a series of MOFs with different doping levels show a decrease in both of the decay components of the Ru^{II}* emission with increased doping (Table 1), consistent with greater quenching of the Ru^{II}* at higher Os^{II} concentrations.

An estimate of the Ru*−Ru hopping time and transport distance can be made from the dependence of the time-resolved emission data on Os loading. Since there is a finite diffusion distance of the

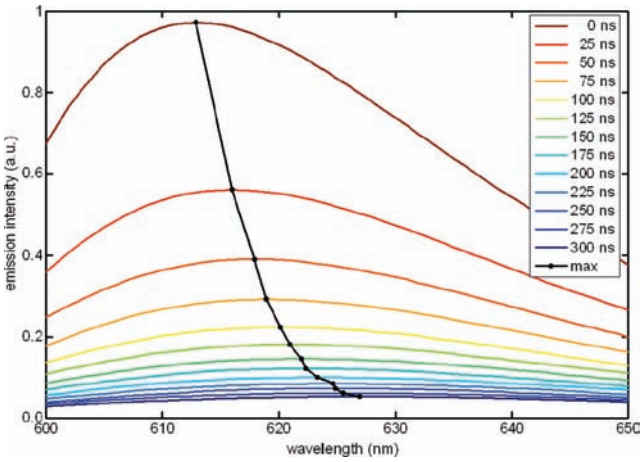

Figure 4. Reconstructed $\mathbf{L_{Ru}}$Zn MOF time-resolved emission spectra demonstrating a dynamic red shift. Solid color lines indicate stretched Gaussian fits of experimental data. The black line designates the wavelength maximum for each time slice fit. Experimentally collected emission spectra time slices can be found in Figure S10.

Ru* excited state during its lifetime, each Os complex will have a radius (R_Q) in which energy transfer quenching of a Ru* can occur before excited state deactivation. At sufficiently low Os concentrations, the average distance between Os^{II} complexes will exceed this quenching radius and the Os^{II} and Ru^{II} emission kinetics will be independent of Os loading. At higher Os levels there will be sufficient overlap between the quenching radii of the Os complexes that a given excited state could be quenched by more than one Os trap, resulting in a faster growth and subsequent decay of the Os emission, as well as a faster decay of the Ru^{II}* emission.

Our time-resolved data (Table 1 and Figure S12) show a dependence on the Os^{II} concentration, even at the lowest Os concentrations studied, suggesting that for doping levels in the range of 0.3 to 0.6 mol % Os the quenching radii are starting to overlap. By taking the midpoint concentration, we can estimate that there are approximately 225 Ru complexes contained within the quenching radius. The number of hops needed to reach the trap will depend upon connectivity and whether energy migration is isotropic (3D) or restricted to a bilayer (2D). Analysis of the crystal structure indicates that, for 3D migration, these 225 complexes surrounding the trap would occupy a sphere with a radius of ~40 Å, whereas a quenching radius of ~75 Å is obtained if energy transport is restricted to a bilayer (i.e., 2D). Considering the migration process to be a random walk, the number of hops needed to traverse this distance is approximated to be $N_{Ru-Ru} = (R_Q/\sigma_{EnT})^2$, where σ_{EnT} is the distance traveled per hop. Taking $\sigma_{EnT} \approx 10$ Å, the nearest neighbor distance, we estimate that on average an excited state will make between 15 and 55 hops during its lifetime (~375 ns for the red edge of the Ru^{II} emission), the lower and upper limits corresponding to 3D and 2D migration, respectively. The corresponding average hopping times are in the range of 25 ns (for 3D migration) to 7 ns (for 2D migration). The actual migration is likely anisotropic with transport within a single layer and between layers occurring at different rates. More sophisticated modeling is needed to discern the relative importance of the 3D and 2D migration pathways. We are currently pursuing stochastic kinetic simulations to model the complex energy transport dynamics.

Our results are important in demonstrating rapid, efficient energy migration and long distance transfer in isomorphous MOFs with mixed $\{M[4,4'\text{-}(HO_2C)_2\text{-bpy}]_2\text{bpy}\}^{2+}$ (M = Ru or Os) building blocks. The synthetic tunability of MOFs should allow for the design of other model systems for studying energy transfer dynamics in well-defined crystalline solids to provide new insights into efficient energy migration and transfer pathways in artificial light-harvesting systems.

Acknowledgment. We thank the UNC EFRC: Solar Fuels and Next Generation Photovoltaics, funded by the U.S. Department of Energy (DE-SC0001011); NSF DMR-0906662 for supporting C.A.K. and L.M. (W.L.) and NSF CHE-0809045 for supporting B.P.M. (J.M.P.). C.A.K. is a Carolina Energy Fellow. We also thank Kathryn deKrafft and Danielle Herrod for experimental help.

Supporting Information Available: Experimental procedures and characterization data. This material is available free of charge via the Internet at http://pubs.acs.org.

References

(1) Cheng, Y.-C.; Fleming, G. R. *Annu. Rev. Phys. Chem.* **2009**, *60*, 241.
(2) Aratani, N.; Kim, D.; Osuka, A. *Acc. Chem. Res.* **2009**, *42*, 1922.
(3) (a) Sykora, M.; Maxwell, K. A.; DeSimone, J. M.; Meyer, T. J. *Proc. Natl. Acad. Sci. U.S.A.* **2000**, *97*, 7687–7691. (b) Balzani, V.; Bergamini, G.; Ceroni, P.; Voegtle, F. *Coord. Chem. Rev.* **2007**, *251*, 525.
(4) Wasielewski, M. R. *Acc. Chem. Res.* **2009**, *42*, 1910.
(5) Ward, M. D.; Barigelletti, F. *Coord. Chem. Rev.* **2001**, *216−217*, 127.
(6) Fleming, C. N.; Maxwell, K. A.; DeSimone, J. M.; Meyer, T. J.; Papanikolas, J. M. *J. Am. Chem. Soc.* **2001**, *123*, 10336.
(7) (a) Fleming, C. N.; Jang, P.; Meyer, T. J.; Papanikolas, J. M. *J. Phys. Chem. B* **2004**, *108*, 2205. (b) Odobel, F.; Massiot, D.; Harrison, B. S.; Schanze, K. S. *Langmuir* **2003**, *19*, 30. (c) Devenney, M.; Worl, L. A.; Gould, S.; Guadalupe, A.; Sullivan, B. P.; Caspar, J. V.; Leasure, R. L.; Gardner, J. R.; Meyer, T. J. *J. Phys. Chem. A* **1997**, *101*, 4535. (d) Trammell, S. A.; Yang, J.; Sykora, M.; Fleming, C. N.; Odobel, F.; Meyer, T. J. *J. Phys. Chem. B* **2001**, *105*, 8895.
(8) (a) Tsushima, M.; Ikeda, N.; Yoshimura, A.; Nozaki, K.; Ohno, T. *Coord. Chem. Rev.* **2000**, *208*, 299. (b) Ikeda, N.; Yoshimura, A.; Tsushima, M.; Ohno, T. *J. Phys. Chem. A* **2000**, *104*, 6158. (c) Tsushima, M.; Ikeda, N.; Nozaki, K.; Ohno, T. *J. Phys. Chem. A* **2000**, *104*, 5176. (d) Breu, J.; Kratzer, C.; Yersin, H. *J. Am. Chem. Soc.* **2000**, *122*, 2548. (e) Yersin, H.; Kratzer, C. *Chem. Phys. Lett.* **2002**, *362*, 365. (f) Yersin, H.; Kratzer, C. *Coord. Chem. Rev.* **2002**, *229*, 75.
(9) (a) Higgins, G. T.; Bergeron, B. V.; Hasselmann, G. M.; Farzad, F.; Meyer, G. J. *J. Phys. Chem. B* **2006**, *110*, 2598. (b) Ardo, S.; Meyer, G. J. *Chem. Soc. Rev.* **2009**, *38*, 115.
(10) (a) Rowsell, J. L. C.; Yaghi, O. M. *Angew. Chem., Int. Ed.* **2005**, *44*, 4670. (b) Kitagawa, S.; Kitaura, R.; Noro, S. *Angew. Chem., Int. Ed* **2004**, *43*, 2334. (c) Wu, C.-D.; Hu, A.; Zhang, L.; Lin, W. *J. Am. Chem. Soc.* **2005**, *127*, 8940. (d) Lee, J. Y.; Farha, O. K.; Roberts, J.; Scheidt, K. A.; Nguyen, S. B. T.; Hupp, J. T. *Chem. Soc. Rev.* **2009**, *38*, 1450. (e) Huxford, R. C.; Della Rocca, J.; Lin, W. *Curr. Opin. Chem. Biol.* **2010**, *14*, 262. (f) Ferey, G.; Mellot-Draznieks, C.; Serre, C.; Millange, F. *Acc. Chem. Res.* **2005**, *38*, 217.
(11) Evans, O. R.; Lin, W. *Acc. Chem. Res.* **2002**, *35*, 511.
(12) (a) Allendorf, M. D.; Bauer, C. A.; Bhakta, R. K.; Houk, R. J. T. *Chem. Soc. Rev.* **2009**, *38*, 1330. (b) Chen, B.; Wang, L.; Xiao, Y.; Fronczek, F. R.; Xue, M.; Cui, Y.; Qian, G. *Angew. Chem., Int. Ed.* **2009**, *48*, 500. (c) Xie, Z.; Ma, L.; deKrafft, K. E.; Jin, A.; Lin, W. *J. Am. Chem. Soc.* **2010**, *132*, 922. (d) Rieter, W. J.; Taylor, K. M. L.; Lin, W. *J. Am. Chem. Soc.* **2007**, *129*, 9852.
(13) (a) Lin, W.; Rieter, J. W.; Taylor, K. M. L. *Angew. Chem., Int. Ed.* **2009**, *48*, 650. (b) Della Rocca, J.; Lin, W. *Eur. J. Inorg. Chem.* **2010**, 3725.
(14) (a) Kalyanasundaram, K.; Nazeeruddin, M. K. *Chem. Phys. Lett.* **1992**, *193*, 292. (b) Nazeeruddin, M. K.; Kalyanasundaram, K. *Inorg. Chem.* **1989**, *28*, 4251.
(15) (a) Meyer, T. J. *Pure Appl. Chem.* **1986**, *58*, 1193. (b) Demadis, K. D.; Dattelbaum, D. M.; Kober, E. M.; Concepcion, J. J.; Paul, J. J.; Meyer, T. J.; White, P. S. *Inorg. Chim. Acta* **2007**, *360*, 1143. (c) Kumaresan, D.; Shankar, K.; Vaidya, S.; Schmehl, R. H. *Top. Curr. Chem.* **2007**, *281*, 101.
(16) Although not measured in the $\mathbf{L_M}$Zn MOFs here, the ratio of quantum efficiencies of $Ru(bpy)_3^{2+}/Os(bpy)_3^{2+}$ is on the order of 10:1. Fetterolf, M. L.; Offen, H. W. *J. Phys. Chem.* **1985**, *89*, 3320.
(17) The excitation beam is reflected off a dichroic mirror (R: 850−1100 nm, T: 450−780 nm) into the objective (Olympus MSPlan 50×, NA 0.8) of an inverted microscope. Backscattered emission collected by the objective is transmitted through the beamsplitter, focused onto the entrance slit of a monochromator, and detected by a photomultiplier tube operated in a time correlated single photon counting scheme. The diameter of the excitation region is estimated to be ~350 nm. The instrument response function of the system is ~100 ps.

JA102804S